JOURNAL OF AIRCRAFT
Vol. 34, No. 1, January–February 1997

Numerical Procedure for the Dynamic Analysis of Three-Dimensional Aeronautical Structures

Silvano Tizzi*
University of Rome "La Sapienza," Rome 00184, Italy

A numerical procedure, which arises from the Rayleigh–Ritz method, previously applied for the dynamic analysis of plane aeronautical structures, has been used for the computation of frequencies and vibration modes of the same structures, but formed by bidimensional component elements in a three-dimensional space. The structural components may be typical parts of wings or tail surfaces in different planes. The expressions of the strain and kinetic energy, corresponding to both in-plane and out-of-plane elastic behavior, have been written. From these, by utilizing polynomial power series expansions for the independent variables, it is possible to evaluate the stiffness and mass matrices by an analytical rather than numerical method. Then from the Hamilton's principle, imposing the stationary conditions of the total energy leads to the generalized eigenvalue problem, whose solution is found by an appropriate algorithm. A comparison of the obtained results with those of the finite element method program MSC/NASTRAN has been performed to better understand the convergence rate of the proposed method.

Nomenclature

A	=	membrane rigidity modulus
D	=	bending stiffness modulus
E	=	Young's modulus
E_{12}, E_ν	=	elastic parameters containing the Young's modulus
G	=	shear modulus
h	=	plate thickness
J	=	inertia moment of the plate thickness per unity surface
K	=	stiffness matrix
L	=	spanwise plate length
L_0	=	reference length
M	=	mass matrix
N	=	number of Lagrangian degrees of freedom
$n_{\nu 2}$	=	elastic parameter containing Poisson's ratio
P, P_i	=	polynomial with its first derivative
P_{ijn}, P_{uPn}, P_{Pn}	=	integrals evaluated in the plate surface
q_i	=	generic Lagrangian degree of freedom
S	=	plate surface
$\mathcal{T}$	=	kinetic energy
U, V, W	=	nondimensional displacements along the main reference system coordinates
$\mathcal{U}_f$	=	flexural and torsional strain energy
$\mathcal{U}_p$	=	in-plane strain energy
$\mathcal{U}_T$	=	total strain energy
$\mathcal{U}_V$	=	shear strain energy
u, v, w; u_1, u_2, u_3	=	displacements along the main reference system coordinates
u_l, v_l, w_l; u_{l1}, u_{l2}, u_{l3}	=	displacements along the plate local reference system coordinates
X, Y, Z; X_1, X_2, X_3	=	nondimensional coordinate of the main reference system
x, y, z; x_1, x_2, x_3	=	main reference system
x^*, y^*, z^*	=	utilized reference system
x_l, y_l, z_l; x_{l1}, x_{l2}, x_{l3}	=	plate local reference system
x_0, y_0, z_0; x_{01}, x_{02}, x_{03}	=	coordinates of the local reference system center
α, β, γ	=	Euler's angles
Δ	=	parameter having a quadratic chordwise variation
Δ_0, Δ_1, Δ_2	=	coefficients of $\Delta(\eta)$ quadratic expansion
δ_{ij}	=	Kronecker's delta
ξ, η	=	plate natural reference system
θ_{l1}, θ_{l2}; θ_Y, $-\theta_X$	=	rotations around the plate local reference system coordinates x_l, y_l
θ_1, θ_2, θ_3; θ_x, θ_y, θ_z	=	rotations around the main reference system coordinates x, y, z
Λ_0	=	leading-edge sweep angle
ν	=	Poisson's ratio
ρ	=	mass density
ω	=	angular frequency
ω_d	=	nondimensional angular frequency parameter

Subscripts

$i_k j_l$	=	elements of the mass or stiffness matrix corresponding to the Lagrangian degrees of freedom q_{i_k} and q_{j_l}
T	=	transpose of the matrix ( )

Introduction

A NUMERICAL procedure,[1–3] which lies between the Rayleigh–Ritz method[4–6] and the finite element method (FEM)[7,8] and which can be obtained combining the Ritz analysis with the variational principles[9–11] (like FEM), is applied to aircraft structures formed by bidimensional plate elements in a three-dimensional space.

In this method we utilize equivalent isotropic plates of the Mindlin model[12,13] to simulate the dynamic behavior of the structural component elements, and consequently, the internal elements of the aircraft structure (like spars, ribs, etc.) are not considered.

Other authors have applied the Rayleigh–Ritz method or the FEM to approach a similar plate analysis formulation or used more complex equivalent plate models, which are useful to

Received Dec. 30, 1994; revision received Oct. 15, 1996; accepted for publication Oct. 28, 1996.

*Researcher, Aerospace Department.

simulate the static or dynamic behavior of aircraft structures component elements.

Giles[14,15] built a numerical approach from the Ritz method, which considers an aircraft wing as being formed by a multiple series of equivalent trapezoidal segments [as in the proposed method (PM)], and it is very realistic in simulating the true internal structure of aircraft wings. He didn't consider the possibility of shear vibration modes, according to the Kirchhoff theory.[16] An equally realistic numerical model was built by Livne,[17] which took into account the possibility of transverse shear strain in the equivalent plate analysis formulation.

Liew and Lim[18] and Liew et al.[19] were interested in the study of the dynamic vibration analysis of trapezoidal plates, with a spanwise linear thickness variation and no chordwise variation. Their dynamic analysis didn't consider shear and in-plane vibration modes.

The same Liew et al.[20] utilized the Rayleigh–Ritz method for a study of the dynamic behavior of skew plates, where also the possibility of shear strain was considered according to the Mindlin model and with constant plate thickness. A similar analysis with the FEM was performed by McGee and Butalia,[21] where also the possibility of in-plane vibration was taken into account.

Jaunky et al.[3] applied this procedure for a study of static buckling behavior of anisotropic skew thick plates and an identical method was used to form the stiffness matrix.

The previously mentioned authors developed good and interesting numerical models, which gave rise to this utilized method. However none of them proposed a realistic way of approaching the dynamic behavior of a set of structural component plate elements in different planes, starting from the Rayleigh–Ritz method and without utilizing FEM. Also in the Giles[14,15] model the plate trapezoidal elements lie on the same plane.

As in the FEM there is a local reference system, where the independent variables, displacements and rotations, are introduced and defined. Also, the structural operators and the constitutive equations are referred to this coordinate system. Since no grid points exist in the PM, for continuity of all the independent variables it is necessary to utilize describing functions, defined in the global reference system. This gives rise to a computational problem because it is necessary to transfer all of the independent variables and the structural operators into the global coordinate system before the numerical algorithm can be started (or vice versa we could transfer everything into the local reference system).

Once the expressions of the strain and kinetic energy vs the Lagrangian degrees of freedom are known, it is possible to form the stiffness and mass matrices, respectively (as in the FEM). Then the stationary conditions of the total energy are imposed by the variational Hamilton's principle[11] and we arrive at the generalized eigenvalue problem, whose solution is found by the subroutine F02BJF of the NAG utility package.[23]

Utilized Reference Systems

First it is necessary to introduce all of the reference systems to have a preliminary idea of the way by which the method has been applied.

A local reference system in the plane of a bidimensional plate x_l, y_l, z_l and another x^*, y^*, z^* are connected via the relations:

$$\begin{aligned} x^* &= x_l \cos\gamma - y_l \sin\gamma \\ y^* &= x_l \sin\gamma + y_l \cos\gamma \\ z^* &= z_l \end{aligned} \tag{1}$$

as can be seen in Fig. 1.

The axis x^* is parallel to the plane x, y of the main reference system x, y, z, and we have the following relations:

$$\begin{aligned} x &= x_0 + x^* \cos\alpha - y^* \sin\alpha \cos\beta \\ y &= y_0 + x^* \sin\alpha + y^* \cos\alpha \cos\beta \\ z &= z_0 + y^* \sin\beta \end{aligned} \tag{2}$$

as in Fig. 2.

From the relations (1) and (2) we have the main reference system in terms of the local reference system

$$x_i = x_{0i} + R_{ij} x_{lj} \qquad j = 1, 2 \quad i = 1, 2, 3 \tag{3a}$$

where

$$\begin{aligned} &x_1 = x \qquad x_2 = y \qquad x_3 = z \qquad x_{l1} = x_l \\ &x_{l2} = y_l \qquad x_{01} = x_0 \qquad x_{02} = y_0 \qquad x_{03} = z_0 \end{aligned} \tag{3b}$$

and the coefficients R_{ij} are the rotation matrix elements

$$\begin{aligned} R_{11} &= \cos\gamma\cos\alpha - \cos\beta\sin\alpha\sin\gamma \\ R_{12} &= -\cos\alpha\sin\gamma - \sin\alpha\cos\beta\cos\gamma \\ R_{21} &= \sin\alpha\cos\gamma + \cos\alpha\cos\beta\sin\gamma \\ R_{22} &= \cos\alpha\cos\beta\cos\gamma - \sin\alpha\sin\gamma \\ R_{31} &= \sin\beta\sin\gamma \qquad R_{32} = \sin\beta\cos\gamma \end{aligned} \tag{3c}$$

For the computation of the integrals occurring in the numerical

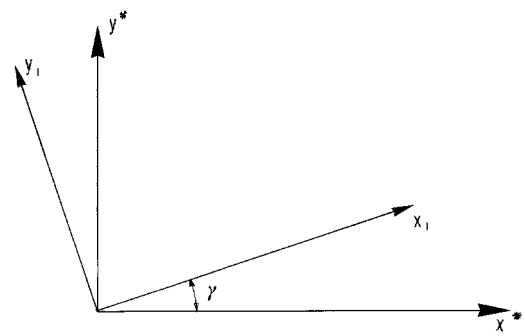

Fig. 1 Two systems of oriented axes x_l, y_l and x^*, y^*.

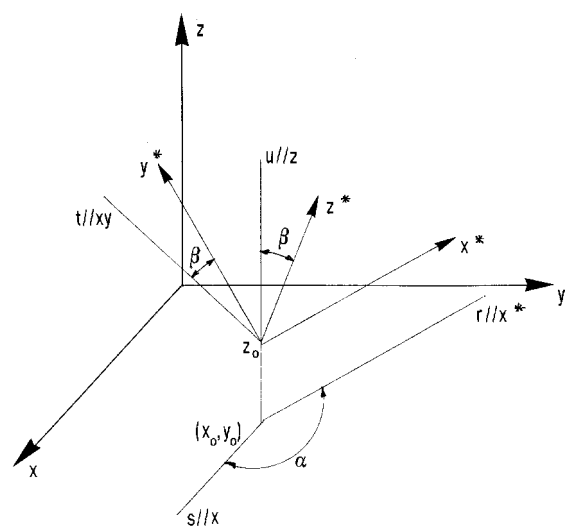

Fig. 2 Reference system x^*, y^*, z^* and the main reference system x, y, z. (The symbol // means parallel to.)

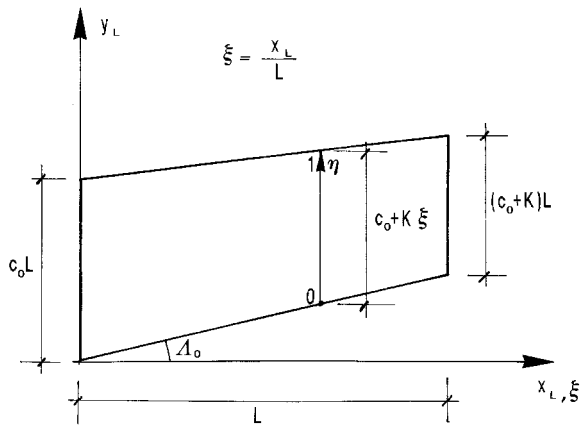

Fig. 3 Natural reference system ξ, η with the local reference system x_l, y_l.

algorithms it is useful to introduce a natural reference system ξ, η ($0 \leq \xi, \eta \leq 1$), as shown in Fig. 3.

The natural and local reference systems are connected via the relations

$$\begin{aligned} x_l &= L\xi \\ y_l &= c(x_l)\eta + \tan(\Lambda_0)x_l \end{aligned} \tag{4}$$

and if we suppose that the chord length $c(x_l)$ is equal to

$$c(x_l) = (c_0 + k\xi)L \tag{5}$$

we obtain the same relations already utilized by Santini et al.[22]:

$$\begin{aligned} x_l &= C_1\xi \\ y_l &= C_2\xi + C_3\eta + C_4\xi\eta \end{aligned} \tag{6a}$$

where

$$C_1 = L \qquad C_2 = L\tan\Lambda_0 \qquad C_3 = c_0L \qquad C_4 = kL \tag{6b}$$

By the introduced reference systems it is possible to compute the integrals analytically, the knowledge of which is indispensable to form the stiffness and mass matrices.

Mathematical Model

The flexural and torsional strain energy expression[20] can be written in the form

$$\mathcal{U}_f = \frac{1}{2}\int_S D\left[\left(\frac{\partial\theta_X}{\partial x_l}\right)^2 + \frac{1-\nu}{2}\left(\frac{\partial\theta_X}{\partial y_l} + \frac{\partial\theta_Y}{\partial x_l}\right)^2 + \left(\frac{\partial\theta_Y}{\partial y_l}\right)^2 + 2\nu\left(\frac{\partial\theta_X}{\partial x_l}\right)\left(\frac{\partial\theta_Y}{\partial y_l}\right)\right]\mathrm{d}S \tag{7}$$

where θ_X and θ_Y are the rotations around the axes $-y_l$ and x_l, respectively, and the shear strain energy can be written as

$$\mathcal{U}_V = \frac{1}{2}G\int_S h\left[\left(\frac{\partial w_l}{\partial x_l} - \theta_X\right)^2 + \left(\frac{\partial w_l}{\partial y_l} - \theta_Y\right)^2\right]\mathrm{d}S \tag{8}$$

where w_l is the displacement along the axis z_l.

The in-plane strain energy expression[16] reads

$$\mathcal{U}_p = \frac{1}{2}\int_S A\left[\left(\frac{\partial u_l}{\partial x_l}\right)^2 + \frac{1-\nu}{2}\left(\frac{\partial u_l}{\partial y_l} + \frac{\partial v_l}{\partial x_l}\right)^2 + \left(\frac{\partial v_l}{\partial y_l}\right)^2 + 2\nu\left(\frac{\partial u_l}{\partial x_l}\right)\left(\frac{\partial v_l}{\partial y_l}\right)\right]\mathrm{d}S \tag{9a}$$

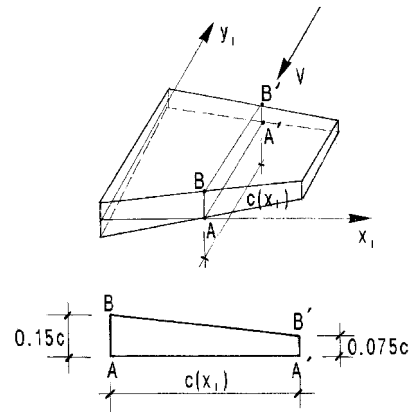

Fig. 4 Thickness chordwise behavior.

where u_l and v_l are the displacements along the axes x_l and y_l, respectively. We have

$$D = \frac{Eh^3}{12(1-\nu^2)} \qquad G = \frac{E}{2(1+\nu)} \qquad A = \frac{Eh}{(1-\nu^2)} \tag{9b}$$

where the expression of h vs ξ and η reads

$$h = c(\xi)\Delta(\eta) \tag{10a}$$

and $\Delta(\eta)$ is a nondimensional parameter for which a chordwise quadratic variation is assumed

$$\Delta(\eta) = \Delta_0 + \Delta_1\eta + \Delta_2\eta^2 \tag{10b}$$

The rotations θ_X and θ_Y are related to the corresponding θ_x, θ_y, and θ_z around the axes x, y, and z, respectively, via the relations

$$\theta_{li} = R_{ji}\theta_j \qquad j = 1, 2, 3 \quad i = 1, 2 \tag{11a}$$

where

$$\theta_{l1} = \theta_Y \qquad \theta_{l2} = -\theta_X \qquad \theta_1 = \theta_x \qquad \theta_2 = \theta_y \qquad \theta_3 = \theta_z \tag{11b}$$

The displacements u_l, v_l, and w_l are related to the corresponding u, v, and w along the axes x, y, and z, respectively, via the relations

$$u_{li} = R_{ji}u_j \qquad j = 1, 2, 3 \quad i = 1, 2, 3 \tag{12a}$$

where

$$\begin{aligned} u_{l1} &= u_l \qquad u_{l2} = v_l \qquad u_{l3} = w_l \\ u_1 &= u \qquad u_2 = v \qquad u_3 = w \end{aligned} \tag{12b}$$

and the other three elements of the rotation matrix are

$$\begin{aligned} R_{13} &= \sin\alpha\sin\beta \\ R_{23} &= -\cos\alpha\sin\beta \\ R_{33} &= \cos\beta \end{aligned} \tag{13}$$

The local displacements u, v, and w can be reformulated in a nondimensional manner with respect to L_0

$$U = u/L_0 \qquad V = v/L_0 \qquad W = w/L_0 \tag{14a}$$

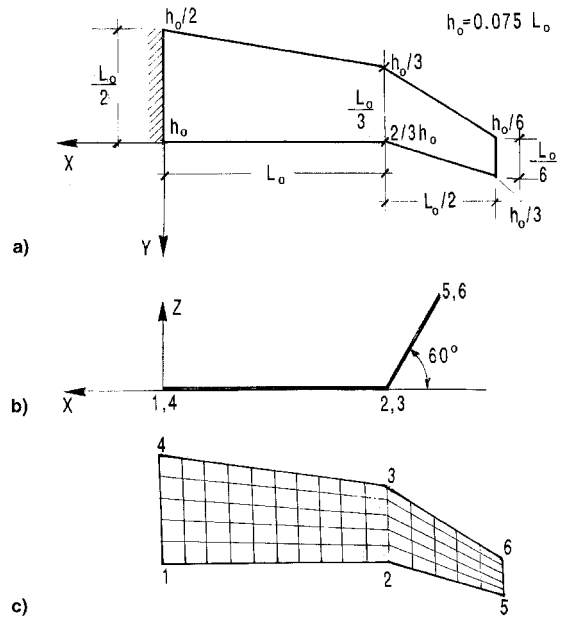

Fig. 5 a) Flattened structure, b) true positioning of the plates, and c) grid mesh of the utilized FEM model.

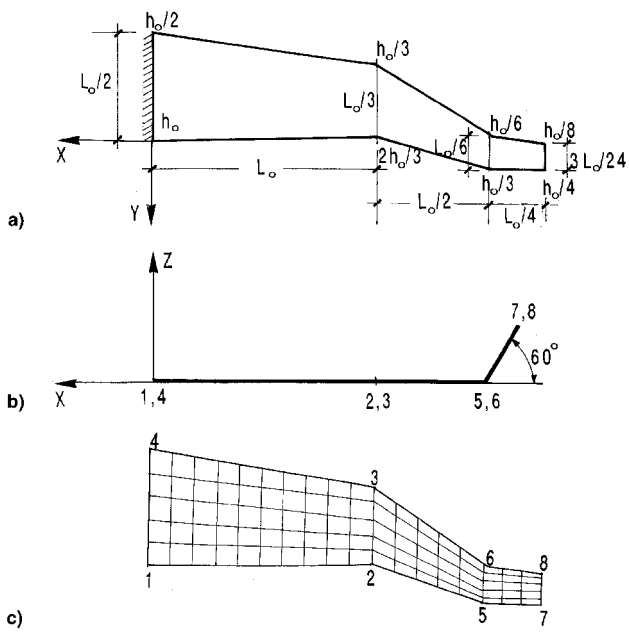

Fig. 6 a) Flattened structure, b) true positioning of the plates, and c) grid mesh of the utilized FEM model.

and also the coordinates x, y, and z can be written in nondimensional form

$$X = x/L_o \qquad Y = y/L_o \qquad Z = z/L_o \tag{14b}$$

The chosen independent variables are U, V, W, θ_x, θ_y, and θ_z, for which the series expansions in sums of polynomial functions read

$$U = \sum_{i_a i_b i_c} U_{i_a i_b i_c} X^{i_a} Y^{i_b} Z^{i_c} \qquad V = \sum_{i_a i_b i_c} V_{i_a i_b i_c} X^{i_a} Y^{i_b} Z^{i_c}$$
$$W = \sum_{i_a i_b i_c} W_{i_a i_b i_c} X^{i_a} Y^{i_b} Z^{i_c} \tag{15a}$$

$$\theta_x = \sum_{i_a i_b i_c} \theta_{x,i_a i_b i_c} X^{i_a} Y^{i_b} Z^{i_c} \qquad \theta_y = \sum_{i_a i_b i_c} \theta_{y,i_a i_b i_c} X^{i_a} Y^{i_b} Z^{i_c}$$
$$\theta_z = \sum_{i_a i_b i_c} \theta_{y,i_a i_b i_c} X^{i_a} Y^{i_b} Z^{i_c} \tag{15b}$$

The independent variables are substituted into the expres-

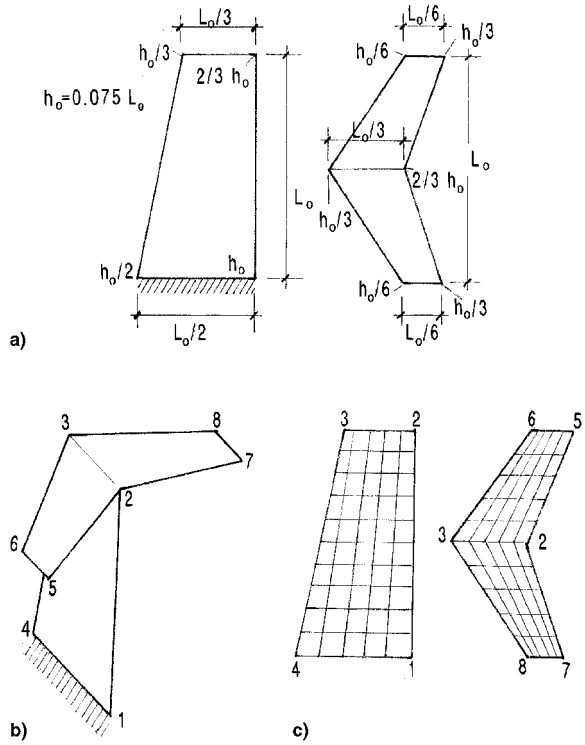

Fig. 7 a), b) Tail structure in the third considered case, together with c) a grid mesh of the utilized FEM model.

Table 1 Vibration frequencies obtained in the first case

Numerical parameters	PM	PM	PM	PM	CV	FEM	FEM
N[a]	180	240	300	360	——	144	164
CPU second[a]	7.0	17.9	36.0	64.8	——	2.1	2.7
First VM[a]	0.04362	0.04355	0.04351	0.04350	0.04349	0.04228	0.04288
Second VM[a]	0.1338	0.1326	0.1318	0.1316	0.1314	0.1256	0.1258
Third VM[a]	0.1603	0.1588	0.1581	0.1578	0.1570	0.1480	0.1500
N[b]	184	305	456	1044	1661	3616	——
CPU second[b]	2.9	4.8	10.3	16.5	28.3	73.0	——
First VM[b]	0.04288	0.04316	0.04328	0.04340	0.04345	0.04347	0.04349
Second VM[b]	0.1259	0.1285	0.1297	0.1308	0.1311	0.1313	0.1314
Third VM[b]	0.1500	0.1530	0.1545	0.1561	0.1566	0.1568	0.1570

[a]Obtained by PM and FEM vs N. [b]Obtained by FEM vs N.

sions of the flexural–torsional shear and in-plane energy, which can be determined by utilizing the relations:

$$\frac{\partial[\,]}{\partial x_{ti}} = R_{ji}\frac{\partial[\,]}{\partial x_j} \qquad j = 1, 2, 3 \quad i = 1, 2 \tag{16}$$

Then the total strain energy $\mathcal{U}_T$

$$\mathcal{U}_T = \mathcal{U}_f + \mathcal{U}_V + \mathcal{U}_p \tag{17}$$

can be written as

$$\mathcal{U}_T = \tfrac{1}{2}\boldsymbol{Q}_T K \boldsymbol{Q} \tag{18}$$

where $\boldsymbol{Q}$ is the column vector of q_i, i.e., the coefficients of the polynomial series expansions [Eqs. (15a) and (15b)].

We can determine the elements of the stiffness matrix as follows:

$$k_{ij} = \frac{\partial^2 \mathcal{U}_T}{\partial q_i \partial q_j} \tag{19}$$

as shown in the Appendix. In the same way the total kinetic energy

$$\mathcal{T} = \frac{1}{2}\omega^2\rho\int_S h(u^2 + v^2 + w^2)\,\mathrm{d}S + \frac{1}{2}\omega^2\int_S J(\theta_x^2 + \theta_y^2 + \theta_z^2)\,\mathrm{d}S \tag{20}$$

where $J = \rho h^3/12$ is the inertia moment per unity surface and ω is the angular vibration frequency, can be written as

$$\mathcal{T} = \tfrac{1}{2}\omega^2 Q_T M Q \tag{21}$$

We can determine the elements of M as follows:

$$m_{ij} = \frac{1}{\omega^2}\frac{\partial^2 \mathcal{T}}{\partial q_i \partial q_j} \tag{22}$$

Table 2 FEM numerical test matrix in the first case

N	Spanwise	Chordwise
144	7	3
164	8	3
184	9	3
305	12	4
456	15	5
1044	23	8
1661	30	10
3616	45	15

as shown in the Appendix. Once the stiffness and mass matrices of the single component elements are known, we can assemble and compute the corresponding matrices of the whole structure. Imposing the minimum of the total energy $(\mathcal{U} - \mathcal{T})$ with respect to the degrees of freedom, according to Hamilton's principle,[11] gives the generalized eigenvalue problem

$$(K - \omega^2 M)Q = 0 \tag{23}$$

and by the previously mentioned algorithm it is possible to find the required eigensolution.

Applications

Three different cases have been examined. In every case we suppose a linear chordwise variation, and the thickness at the trailing edge is twice that one at the leading edge, as in Fig. 4.

The first case refers to a wing structure as in Fig. 5.

In Fig. 5a the flattened structure is sketched while the true positioning of the plates in a three-dimensional space is illustrated in Fig. 5b. A sample of the grid mesh utilized in the FEM model is shown in Fig. 5c.

Figure 6 shows the geometry of a different typical aeronautical structure. The first two components elements, which lie on the same plane, are the same as the previous case, but a third element is added at the end of the spanwise wing (which could be a typical winglet).

Likewise, in the previous case the flattened structure is sketched in Fig. 6a and the true positioning of the component elements is reported in Fig. 6b. Also, a sample of the utilized FEM model is shown in Fig. 6c.

In the third considered case, a typical tail structure, formed by three component elements (two lie on the same plane), is shown in Fig. 7. Both the vertical and the two horizontal component elements are sketched in Fig. 7a, while a trimetric drawing of the whole structure is shown in Fig. 7b. A sample of the grid mesh in the utilized FEM is shown in Fig. 7c.

Results

The values of the nondimensional angular frequency parameter

$$\omega_d = \omega^2\rho L_0^2/E$$

corresponding to the different vibration modes (VM) and obtained in the first case both by the PM and by the FEM, utilizing a MSC/NASTRAN program[24] (version 68 and with lumped mass formulation), are reported in Table 1. The plate elements utilized in MSC/NASTRAN program are QUAD4, the thickness of which can vary isoparametrically over the surface. The FEM numerical test matrix, which specifies the number of elements into which the structure is divided spanwise and chordwise in the FEM model, is reported in Table 2. Figure 5c shows the utilized grid mesh in case $N = 456$. The results

Table 3 Vibration frequencies obtained in the second case

Numerical parameters	PM	PM	PM	PM	CV	FEM	FEM
N[a]	180	240	300	360	——	168	204
CPU second[a]	7.1	17.6	35.3	59.5	——	3.8	4.2
First VM[a]	0.0352	0.03516	0.03513	0.03512	0.03511	0.03457	0.03451
Second VM[a]	0.1080	0.1078	0.1075	0.1074	0.10715	0.1036	0.1038
Third VM[a]	0.2161	0.2141	0.2130	0.2126	0.2110	0.1962	0.2006
N[b]	224	355	546	1224	1936	4256	——
CPU second[b]	4.4	6.7	11.1	24.1	42.1	90.2	——
First VM[b]	0.03461	0.03482	0.03493	0.03504	0.03507	0.03509	0.03511
Second VM[b]	0.1038	0.1048	0.1059	0.1066	0.1068	0.1070	0.10715
Third VM[b]	0.2011	0.2008	0.2033	0.2081	0.2091	0.2101	0.2110

[a]Obtained by PM and FEM vs N. [b]Obtained by FEM vs N.

obtained by the FEM as the number of degrees of freedom grows indefinitely, converge approximately toward the value [convergence value (CV)], which is reported in Table 1.

Table 3 shows the same parameter values obtained in the second case also with CV. The corresponding FEM numerical test matrix is written in Table 4. The utilized grid mesh of the FEM model for the case $N = 546$ is sketched in Fig. 6c.

The obtained results of the third case in the frequency parameter and the CV are reported in Table 5, while Table 6 shows the corresponding FEM numerical test matrix (it must be remarked that we report the sum of the spanwise subdivisions of all the component elements, while the number of the chordwise subdivisions is obviously the same in all three elements). The utilized grid mesh when $N = 606$ is shown in Fig. 7c.

To have an insight into the convergence rate of the PM in comparison with the same of the FEM, it is useful to look at the following figures, which give the values of the first frequencies vs $1/N$ in both methods. Figure 8 shows such a behavior in the first considered case, while Figs. 9 and 10 show the same behaviors in the second and third case, respectively, where all of the data points, corresponding to the results of Tables 1, 3, and 5, appear as dots. In the first case, the data points corresponding to the first frequency values obtained by the FEM with $N = 144$ have not been reported because they are much lower than the frequency value corresponding to the abscissa axis. It must be emphasized that for $N > 360$ there are no data points of the PM because of the presence of convergence problems of the utilized eigensolver algorithm, and consequently, such a behavior, sketched by a dashed line, is only presumed to be valid. It has been obtained by polynomial extrapolation, supposing a continuous and regular function beyond the previously mentioned value. We can see that the frequencies obtained by the PM with $N = 300$ or 360 are very near the CV, and it is possible to evince a much higher relative divergence of the results obtained by the FEM for the same values of N. From the same figures one can also notice that many more degrees of freedom are necessary with FEM to obtain as many accurate results as those of the PM.

The behaviors of the second and third frequency values vs $1/N$ are very similar to the previous ones, and for this reason they have not been reported in this paper.

Table 4 FEM numerical test matrix in the second case

N	Spanwise	Chordwise
168	11	2
204	10	3
224	11	3
355	14	4
546	18	5
1224	27	8
1936	35	10
4256	53	15

A comparison of the modal shapes obtained by both methods has to be performed to verify the eigenvectors convergence. In Figs. 11–13 the modal behaviors in the first case corresponding to the first, second, and third frequency, respectively, obtained both by FEM with $N = 456$ and by PM with $N = 240$, are reported. Figures 14–16 show the same modal shape in the second case, obtained by FEM with $N = 546$ and PM with $N = 240$; whereas the modal configurations corresponding to the same frequencies in the third case, obtained by FEM with $N = 606$ and PM with $N = 240$, are sketched in Figs. 17–19. We can see that there is good agreement between the modal shapes of both methods.

Discussion

It is necessary to make a comparison among the three considered cases to point out the difference between them and to explain the reason for which such structures have been chosen. It will then be possible to emphasize the advantages of PM with regard to FEM. The first case is the simplest to be treated for a study of dynamic behavior, because the structure is formed only by two component elements. The second case is a little more complex because there is a third structural element together with two having the same dimensions of the previous case. The third case is the most complex to be treated, because there are three component elements, the third of which has the same dimensions of the second; this is different from the previous case where it was smaller, and the first two component elements are exactly the same as in the two previous cases. Furthermore, the first element is perpendicular to the other two.

From Tables 1–6 notice that in all cases the frequency values obtained by the PM with $N = 300$ are very good and the CPU time is nearly the same. It is not necessary to utilize $N = 360$ degrees of freedom, because the much higher CPU time doesn't justify the little improvement obtained. We can see also that in the first case $N = 3616$ degrees of freedom and a CPU time of $t = 73.0$ s are necessary with FEM to have as many good values as those obtained by the PM with $N = 300$ (i.e., which differ from the CV of about the same quantity) for the first frequency.

In the second case, $N = 4256$ degrees of freedom with a CPU time of $t = 90.2$ s are necessary to have as many good values as those of PM for the first frequency.

In the third considered case, $N = 4816$ degrees of freedom and a CPU time of $t = 106.1$ s are necessary to the FEM program to obtain as many good values as the corresponding ones of the PM for the first frequency and also more for the second frequency.

This is the most interesting aspect of the performed analysis: in every case we can save the core storage requirements (because the PM utilizes a smaller number of Lagrangian degrees of freedom), but also as the structure becomes more complex the advantages of the PM grow, that is, the greater the complexity of the structure becomes, the greater the convenience

Table 5 Vibration frequencies obtained in the third case

Numerical parameters	PM	PM	PM	PM	CV	FEM	FEM
N[a]	180	240	300	360	——	153	224
CPU second[a]	7.3	18.4	37.3	65.7	——	2.9	3.5
First VM[a]	0.03771	0.03764	0.03758	0.03757	0.03756	0.03682	0.03696
Second VM[a]	0.1047	0.1028	0.1022	0.1021	0.1020	0.09211	0.09521
Third VM[a]	0.11768	0.11765	0.1176	0.11757	0.1175	0.1051	0.1128
N[b]	244	405	606	1404	2211	4816	——
CPU second[b]	4.4	7.1	13.6	28.5	48.72	106.1	——
First VM[b]	0.03709	0.03730	0.03740	0.03751	0.03752	0.03754	0.03756
Second VM[b]	0.09587	0.09758	0.09852	0.09945	0.09976	0.1010	0.1020
Third VM[b]	0.1124	0.1147	0.1158	0.1170	0.1172	0.1174	0.1175

[a]Obtained by PM and FEM vs N. [b]Obtained by FEM vs N.

Table 6 FEM numerical test matrix in the third case

N	Spanwise	Chordwise
153	10	2
224	11	3
244	12	3
405	16	4
606	20	5
1404	31	8
2211	40	10
4816	60	15

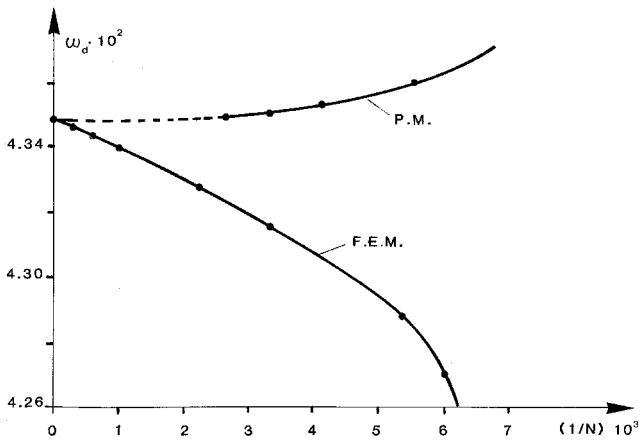

Fig. 8 Behavior of the first frequency vs 1/*N* in the first considered case.

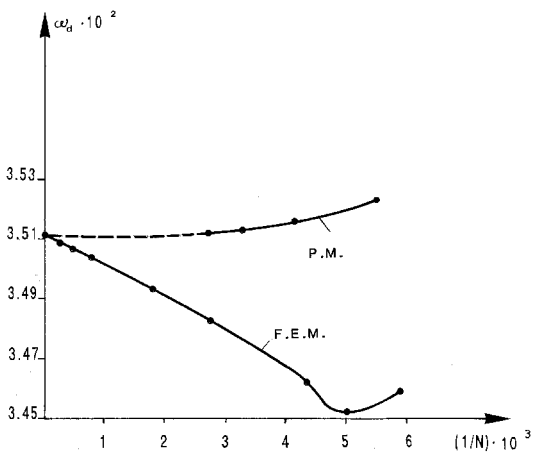

Fig. 9 Behavior of the first frequency vs 1/*N* in the second considered case.

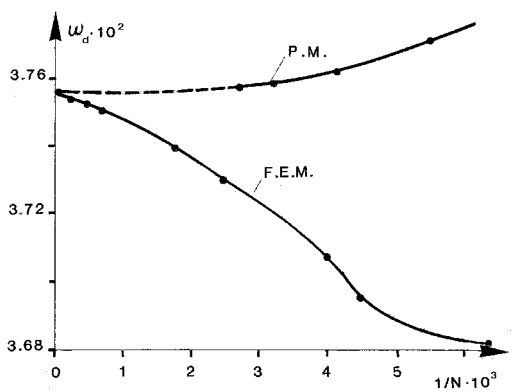

Fig. 10 Behavior of the first frequency vs 1/*N* in the third considered case.

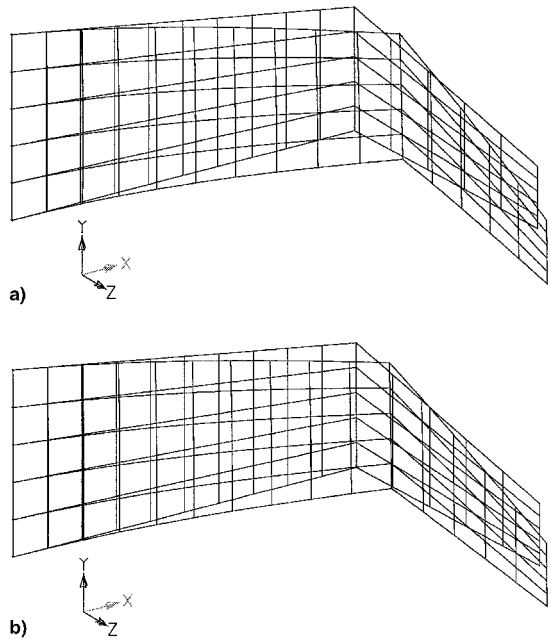

Fig. 11 First flexural mode shape corresponding to the first frequency, obtained in the first case by the FEM with a) *N* = 456 and b) by the PM with *N* = 240.

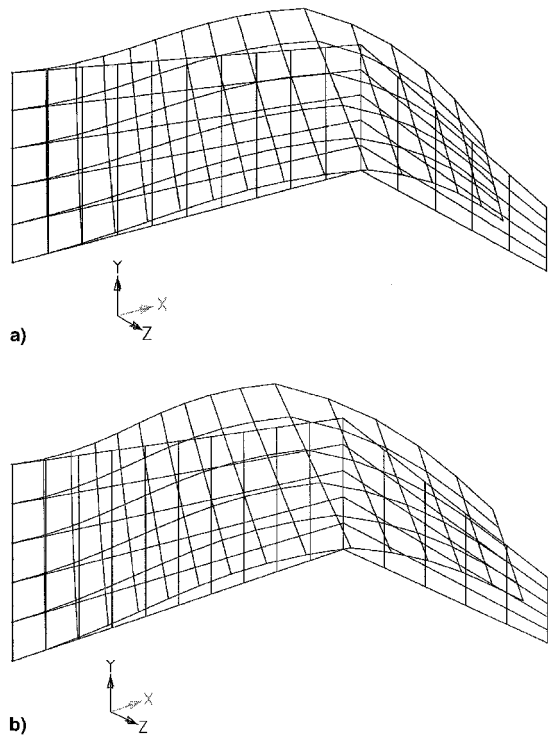

Fig. 12 Second flexural mode shape corresponding to the second frequency, obtained in the first case by the FEM with a) *N* = 456 and b) by the PM with *N* = 240.

in using the P.M., both in terms of the number of degrees of freedom and the CPU time.

This can be explained considering the fact that in case we add other component elements or the dimensions of some of them are increased, other grid points are necessary in the FEM model to have the same resolution, and consequently, the number of describing functions, which are defined in the neighborhood of the grid points, increases as well. For this reason the CPU time also grows. On the contrary, in the PM we utilize describing functions that are defined in all the space containing

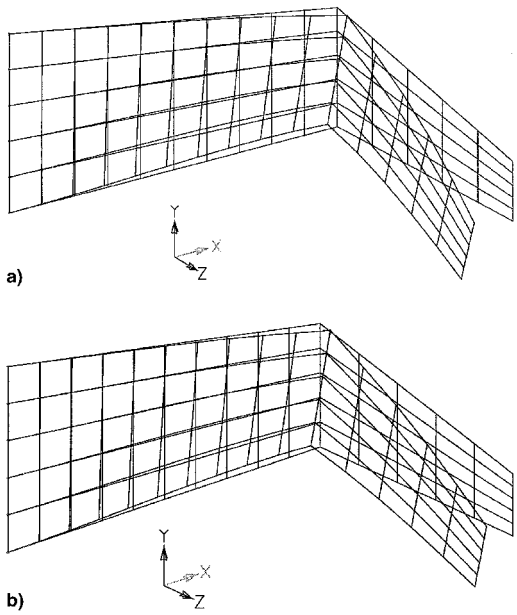

Fig. 13 First torsional mode shape corresponding to the third frequency, obtained in the first case by the FEM with a) $N = 456$ and b) by the PM with $N = 240$.

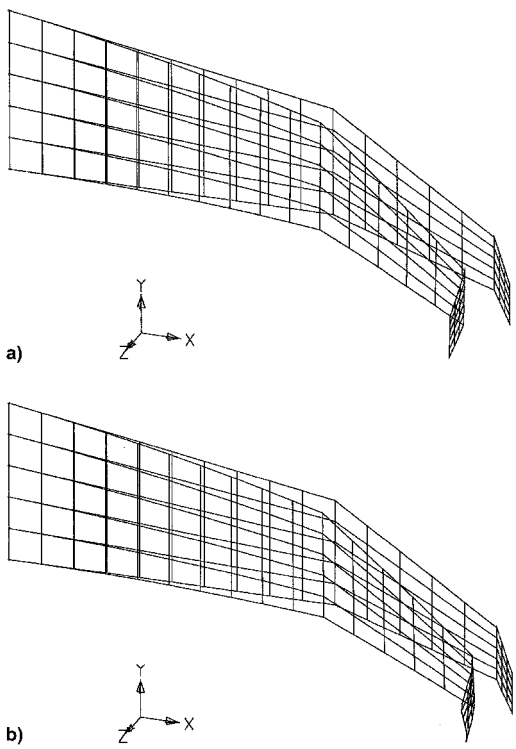

Fig. 14 First flexural mode shape corresponding to the first frequency, obtained in the second case by the FEM with a) $N = 546$ and b) by the PM with $N = 240$.

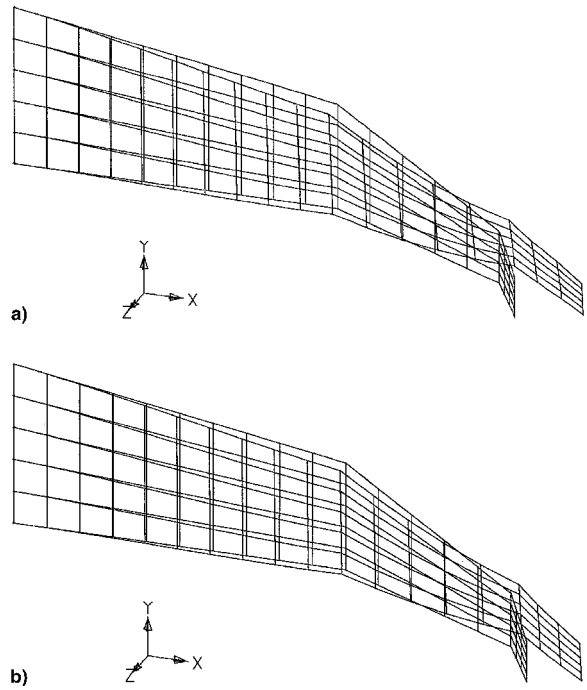

Fig. 15 Second flexural mode shape corresponding to the second frequency, obtained in the second case by the FEM with a) $N = 546$ and b) by the PM with $N = 240$.

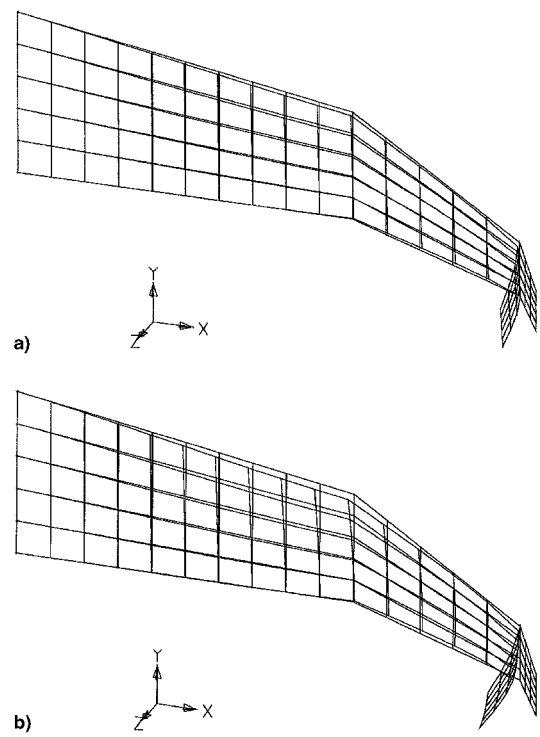

Fig. 16 First torsional mode shape corresponding to the third frequency, obtained in the second case by the FEM with a) $N = 546$ and b) by the PM with $N = 240$.

the structure, including where there are no structural component elements. The same functions with appropriate coefficients in the series expansions can also be utilized when the structure becomes more complex, if we limit our interest to the first vibrating modes.

Furthermore, it must be pointed out that with this numerical program it is possible to find eigensolutions of the dynamic problem in the case of quadratic chordwise variation of the thickness plates, as mentioned in Eq. (10b). Only a linear variation of the thickness has been assumed in the numerical applications, because the MSC/NASTRAN program doesn't allow the dynamic analysis of plates with a nonlinear thickness variation, and consequently, it is not possible to compare the numerical results obtained by the two different procedures.

Unfortunately, there are also limits of the utilized computation model that have to be analyzed and explained. As already mentioned, we suppose the structural elements behave according to the Mindlin plate model, and for this reason the internal structural elements of wings or tail panels, most of

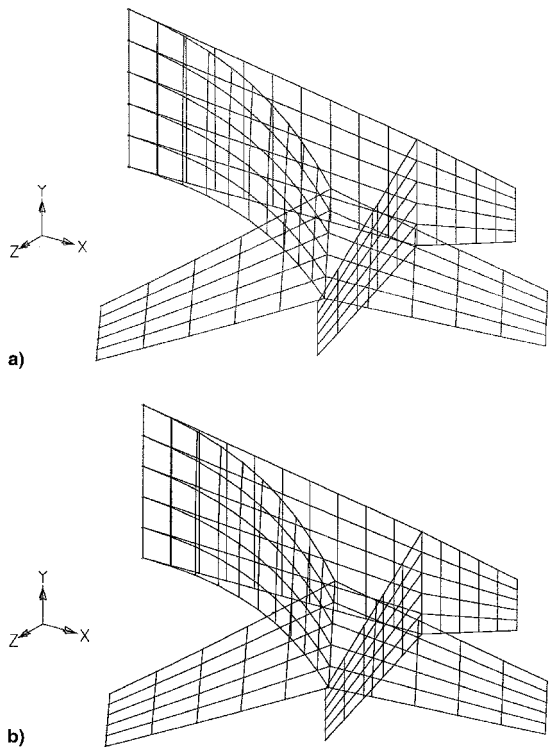

Fig. 17 First flexural mode shape corresponding to the first frequency, obtained in the third case by the FEM with a) $N = 606$ and b) by the PM with $N = 240$.

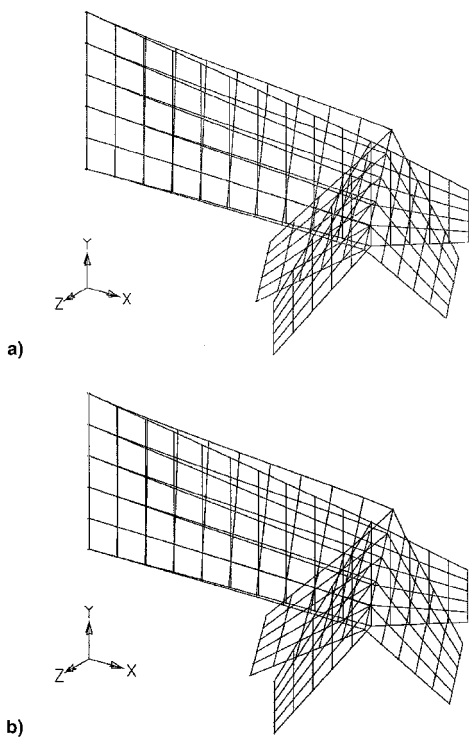

Fig. 18 First torsional mode shape corresponding to the second frequency, obtained in the third case by the FEM with a) $N = 606$ and b) by the PM with $N = 240$.

which are semimonocoque, are not considered. It is not possible by the numerical program utilized to perform the dynamic analysis of fuselages, typical cylindrical structures, and furthermore, it must be emphasized that the present model is not suitable for different and more complicated aircraft structures. Moreover, there are limits because of the particular algorithm of the NAG utility package utilized for the search of the eigensolutions of the dynamic problem. It is not convenient to increase the number N of Lagrangian degrees of freedom beyond the value $N = 360$, because the eigensolver algorithm has trouble converging and no reliable results are obtained.

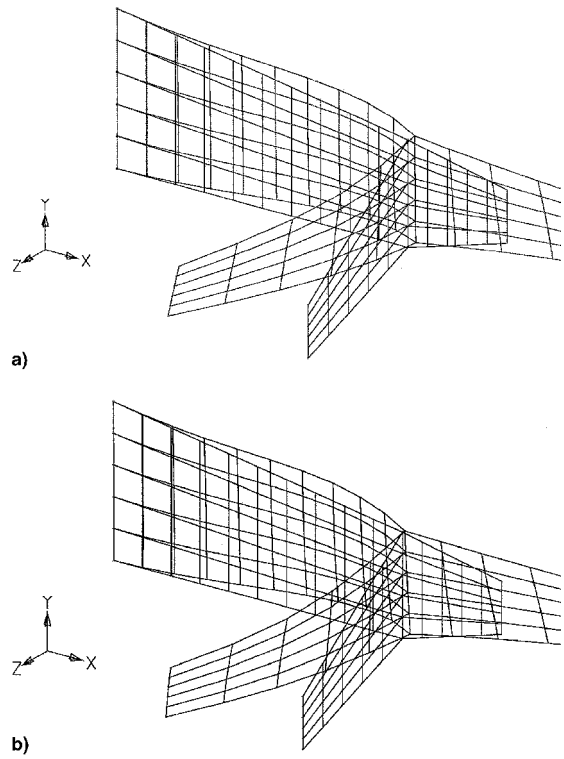

Fig. 19 Second flexural mode shape corresponding to the third frequency, obtained in the third case by the FEM with a) $N = 606$ and b) by the PM with $N = 240$.

However, it must also be emphasized that there is the possibility to properly change the computational model so that it can be made suitable for different and more complicated aircraft structures without having limits for widespread application. Similarly, it would be possible to increase the resolution and the convergence rate of the PM by introducing describing functions, defined only in each single component element by its local coordinates, together with the existing ones in the global reference system.

We can conclude by saying that the utilized method is in progress because the advantages obtained by the introduced procedure are so evident that they can justify future developments of the computational model to extend its applicability to the widest range of aeronautical structures.

Appendix: Evaluation of the Stiffness and Mass Matrices

We introduce the generic polynomial

$$P(l_1, l_2, l_3) = L_0 \prod_{i=1}^{3} X_i^{l_i} \tag{A1}$$

$$P_u(l_1, l_2, l_3) = \frac{\partial P(l_1, l_2, l_3)}{\partial x_{lu}} \qquad u = 1, 2 \tag{A2}$$

We define the integral

$$P_{uvn} = \frac{1}{L_0^{n+2}} \int_S h^n P_u P_v \, \mathrm{d}S \qquad u = 1, 2 \quad v = 1, 2 \tag{A3}$$

and the integral

$$P_{uPn} = \frac{1}{L_0^{n+3}} \int_S h^n P_u(l_1, l_2, l_3) P(m_1, m_2, m_3)\, dS \qquad (A4)$$

At last we introduce the integral

$$P_{Pn} = \frac{1}{L_0^{n+4}} \int_S h^n P(l_1, l_2, l_3) P(m_1, m_2, m_3)\, dS \qquad (A5)$$

Now the stiffness and mass matrices can be determined. First, six couples of subscripts $i_1, j_1 i_2, j_2 i_3, j_3 i_4, j_4 i_5, j_5 i_6, j_6$ corresponding to the variables U, V, W, θ_x, θ_y, θ_z have to be introduced. If N is the number of the Lagrangian degrees of freedom, we have

$$(l - 1)(N/6) < i_l, j_l \leq l(N/6) \qquad l = 1, 2 \ldots 6$$

where

$$\begin{aligned} i_l &= (i_a - 1) \times N_b \times N_c + i_b \times N_c \\ &\quad + i_c + (l - 1) \times (N/6) + 1 \\ j_l &= (j_a - 1) \times N_b \times N_c + j_b \times N_c + j_c \\ &\quad + (l - 1) \times (N/6) + 1 \\ &\quad l = 1, 2 \ldots 6 \end{aligned} \qquad (A6a)$$

where i_a, i_b, and i_c are the exponents of the polynomial series expansions [Eqs. (15a) and (15b)]. Since it is supposed the clamped edge at $x = 0$, it is true that

$$\begin{aligned} &i_a = 1, 2 \ldots N_a \quad i_b = 0, 1, \ldots N_b - 1 \quad i_c = 0, 1 \ldots N_c - 1 \\ &N = 6 N_a N_b N_c \end{aligned} \qquad (A6b)$$

If the relations (11) are substituted into the flexural–torsional strain energy expression (7), taking into account the series expansions (15a) and the expressions (14b) and (16), from the relations (19), we have

$$\begin{aligned} k_{i_l j_m} &= E_{12} L_0^3 [R_{l-3,2} R_{m-3,2} (P_{113} + n_{u2} P_{223}) \\ &\quad - R_{l-3,2} R_{m-3,1} (n_{u2} P_{213} + \nu P_{123}) - R_{l-3,1} R_{m-3,2} (n_{u2} P_{123} \\ &\quad + \nu P_{213}) + R_{l-3,1} R_{m-3,1} (P_{223} + n_{u2} P_{113})] \\ &\quad l, m = 4, 5, 6 \qquad l \leq m \end{aligned} \qquad (A7)$$

where

$$n_{u2} = (1 - \nu)/2 \qquad E_{12} = [E/12(1 - \nu^2)]$$

If the relations (11) and (12) of θ_X, θ_Y, and w_l are substituted into the shear strain energy expression (8), and taking into account the series expansions (15a) and (15b), and the expression (14a), (14b), and (16), from the relations (19), some other elements of the stiffness matrix can be determined

$$k_{i_l j_m} = G L_0^3 R_{l3} R_{m3} (P_{111} + P_{221}) \qquad l, m = 1, 2, 3 \quad l \leq m \qquad (A8)$$

$$\begin{aligned} k_{i_l j_m} &= -G L_0^3 (-R_{l3} R_{m-3,2} P_{1P} + R_{l3} R_{m-3,1} P_{2P}) \\ &\quad l = 1, 2, 3 \quad m = 4, 5, 6 \end{aligned} \qquad (A9)$$

and other contributions to already computed elements

$$\begin{aligned} k_{i_l j_m} &\rightarrow k_{i_l j_m} + G L_0^3 [(R_{l-3,2} R_{m-3,2} + R_{l-3,1} R_{m-3,1}] P_{P1} \\ &\quad l, m = 4, 5, 6 \quad l \leq m \end{aligned} \qquad (A10)$$

If the relations (12) are substituted into the expression (9) of the in-plane strain energy, and also taking into account the series expansions (15a) and the expressions (14a), (14b), and (16), from the relations (19), we find other contributions to the stiffness matrix elements corresponding to U and V:

$$\begin{aligned} k_{i_l j_m} &\rightarrow k_{i_l j_m} + E_v L_0^3 [R_{l1} R_{m1} (P_{111} + n_{u2} P_{221}) \\ &\quad + R_{l1} R_{m2} (n_{u2} P_{211} + \nu P_{121}) + R_{l2} R_{m1} (n_{u2} P_{121} \\ &\quad + \nu P_{211}) + R_{l2} R_{m2} (P_{221} + n_{u2} P_{111})] \\ &\quad l, m = 1, 2, 3 \quad l \leq m \end{aligned} \qquad (A11)$$

where

$$E_v = E/(1 - \nu^2)$$

The symmetry of the stiffness matrix has to be imposed so that also the dual elements of the ones already determined can be found:

$$k_{j_m i_l} = k_{i_l j_m} \qquad l < m \qquad (A12)$$

If the series expansions (15a) and (15b) are substituted into the expression of the kinetic energy (20), and taking into account the expressions (14), from the relations (22) we can determine the mass matrix elements:

$$m_{i_l j_l} = \rho L_0^5 P_{P1} \qquad l = 1, 2, 3 \qquad (A13)$$

$$m_{i_l j_l} = (\rho L_0^5/12) P_{P3} \qquad l = 4, 5, 6 \qquad (A14)$$

References

[1]Tizzi, S., "A Numerical Procedure for the Analysis of a Vibrating Panel in Critical Flutter Conditions," *Computers & Structures*, Vol. 50, No. 3, 1994, pp. 299–316.

[2]Tizzi, S., "Application of a Numerical Procedure for the Dynamic Analysis of Plane Aeronautical Structures," *Journal of Sound and Vibration*, Vol. 193, No. 5, 1996, pp. 957–983.

[3]Juanky, N., Knight, N. F., Jr., Ambur, D. R., "Buckling of Arbitrary Quadrilateral Anisotropic Plates," *AIAA Journal*, Vol. 33, No. 5, 1995, pp. 938–944.

[4]Kantorovich, L. V., and Krylov, V. I., *Approximate Methods of Higher Analysis*, Interscience, New York, 1964, pp. 258–303.

[5]Martin, A. I., and Leissa, A. W., "Application of the Ritz Method to Plane Elasticity Problems for Composite Sheets with Variable Fibre Spacings," *International Journal for Numerical Methods in Engineering*, Vol. 28, No. 8, 1989, pp. 1813–1825.

[6]Reddy, J. N., *Applied Functional Analysis and Variational Methods in Engineering*, McGraw–Hill, New York, 1986, pp. 258–285.

[7]Hughes, T., and Hinton, E., *Finite Elements Methods for Plates and Shells Structures*, Vols. 1 and 2, Pineridge, Swansea, Wales, UK, 1986.

[8]Reddy, J. N., Krishnamoorthy, C. S., and Seetharamu, K. N., *Finite Elements Analysis for Engineering Design*, Springer–Verlag, Berlin, 1988.

[9]Mikhlin, S. G., *Variational Methods in Mathematical Physics*, Pergamon, Oxford, England, UK, 1964, pp. 74–125.

[10]Fichera, G., *Numerical and Quantitative Analysis*, Pitman, London, 1987, pp. 1–12.

[11]Pars, L. A., *A Treatise of Analytical Dynamics*, Books Ltd., Belfast, 1968, pp. 34–37.

[12]Mindlin, R. D., "Influence of Rotary Inertia and Shear in Flexural Motion of Isotropic, Elastic Plates," *Journal of Applied Mechanics*, Vol. 18, No. 1, 1951, pp. 31–38.

[13]Gould, P. L., *Analysis of Shells and Plates*, Springer–Verlag, New York, 1988, pp. 344–346.

[14]Giles, G. L., "Equivalent Plate Analysis of Aircraft Wing Box Structures with General Planform Geometry," *Journal of Aircraft*, Vol. 23, No. 11, 1986, pp. 859–864.

[15]Giles, G. L., "Further Generalization of an Equivalent Plate Representation for Aircraft Structure Analysis," *Journal of Aircraft*, Vol. 26, No. 1, 1989, pp. 67–74.

[16]Santini, P., *Introduzione alla Teoria Delle Strutture*, Tamburini

Editire, Milano, 1973, pp. 294–287, 315–318.

[17]Livne, E., "Equivalent Plate Structural Modeling for Wing Shape Optimization Including Transverse Shear," *AIAA Journal*, Vol. 32, No. 6, 1994, pp. 1278–1288.

[18]Liew, K. M., and Lim, M. K., "Tranverse Vibration of Trapezoidal Plates of Variable Thickness: Symmetric Trapezoids," *Journal of Sound and Vibration*, Vol. 165, No. 1, 1993, pp. 45–67.

[19]Liew, K. M., Lim, C. V., and Lim, M. K., "Transverse Vibration of Trapezoidal Plates of Variable Thickness: Unsymmetric Trapezoids," *Journal of Sound and Vibration*, Vol. 177, No. 4, 1994, pp. 479–501.

[20]Liew, K. M., Xiang, Y., Kitipornchai, S., and Wang, C. M., "Vibration of Thick Skew Plates Based on Mindlin Shear Deformation Plate Theory," *Journal of Sound and Vibration*, Vol. 168, No. 1, 1993, pp. 39–69.

[21]McGee, O. G., and Butalia, T. S., "Natural Vibrations of Shear Deformable Cantilevered Skew Thick Plates," *Journal of Sound and Vibration*, Vol. 176, No. 3, 1994, pp. 351–376.

[22]Santini, P., Sneider, M. A., and Leuzzi, L., "Structural Dynamics of a Cantilever Swept Wing," *L'Aerotecnica, Missili e Spazio*, Vol. 65, No. 3, 1986, pp. 141–149.

[23]"The NAG Fortran Library Manual, Mark 15," NAG Inc., Downers Grove, IL, 1991.

[24]Schaeffer, H. G., "MSC/NASTRAN Primer: Static and Normal Modes, Analysis," Schaeffer Analysis Inc., Mount Vernon, New Hampshire, 1984, pp. 235–240, 360.